Combustion Science and Technology

ISSN: 0010-2202 (Print) 1563-521X (Online) Journal homepage: http://www.tandfonline.com/loi/gcst20

Spherically Symmetric Flame Propagation in Hydrogen-Air Mixtures

G. Dixon-Lewis

Combustion Science and Technology, 1983, Vol. 34, pp. 1–29
0010-2202/83/3406-0001$18.50/0

Spherically Symmetric Flame Propagation in Hydrogen–Air Mixtures

G. DIXON-LEWIS *Department of Fuel and Energy, University of Leeds, Leeds, LS2 9JT, UK*

(*Received May 27, 1983*)

Abstract—A Lagrangian finite difference procedure is outlined for the modelling of constant pressure, spherically symmetric, laminar flames, with detailed chemistry and transport property representation. The procedure is used for modelling spherically expanding hydrogen–air flames such as are obtained during the early, pre-pressure period of constant volume bomb explosions with single spark ignition at the centre. For modelling purposes, such explosions have the advantage over burning velocity measurements on stationary flames that the speeds of radial advance of the flames in space can be measured in a purely objective manner, and they thus provide a calibration standard for the other overall rate processes (such as key reaction rate or diffusion parameters, or indirectly, the burning velocity itself) in the flames.

Sensitivity analyses on the hydrogen–air flame system took full account (a) of published data on the hydrogen–oxygen reaction from a variety of sources, including studies of radical recombination in flames themselves, and (b) of measurements by Clifford, Gray, Mason and Waddicor (1982) of the diffusive properties of hydrogen atoms at room temperature. Taking the "spherical" flame speed of the 41 percent hydrogen–air mixture, measured by Andrews and Bradley (1973), as the calibration standard, they led, for an assumed activation energy $E_2 = 70.3$ kJ mol^{-1}, to a reaction rate coefficient $k_2 = (1.8 \pm 0.2) \times 10^{14} \exp(-8450/T)$ cm^3 mol^{-1} s^{-1} between 700 and 1500 K, where reaction (ii) is:

$$H + O_2 = OH + O \qquad \text{(ii)}$$

Within this range of k_2, complete sets of matched diffusion and reaction rate parameters could be obtained so as to predict the observed flame speed.

Spherical flame speeds predicted with the use of a specific matched set of such parameters agreed well with the measurements of Andrews and Bradley (1973) over the whole flammable range of hydrogen–air mixtures. For an initial temperature of 298 K, the observed flame speeds corresponded with a maximum planar, one-dimensional, laminar hydrogen–air burning velocity of 300 cm s^{-1}, at a composition containing about 41 percent hydrogen. Burning velocities corresponding with other compositions, and a complete matched set of reaction rate and diffusion parameters, are tabulated in the paper. The results were not affected by the inclusion of radiative losses into the calculations.

The flame results do not confine the temperature dependence of k_2 to that of the simple Arrhenius expression above. Retaining the activation energy $E_2 = 70.3$ kJ mol^{-1} as the base, combination of the flame results with recently published shock tube data leads to a three-parameter, modified Arrhenius expression:

$$k_2 = 4.2 \times 10^{15}\, T^{-0.46} \exp(-8450/T),$$

or alternatively:

$$k_2 = 7.8 \times 10^{15}\, T^{-0.55} \exp(-8450/T) \text{ cm}^3 \text{ mol}^{-1} \text{ s}^{-1},$$

over the temperature range from 700 to 2500 K. The expressions have slightly different temperature dependences, but both have confidence limits of ± 10 percent. In the 700 to 1500 K temperature range these limits allow for effects of imprecisions in other key reaction kinetic or diffusion parameters in the context of the flame modelling.

1 INTRODUCTION

A recent discussion by Dixon-Lewis and Islam (1982) of techniques for the measurement of burning velocity concluded with reference to studies of the movement of

non-stationary flames in initially quiescent, flammable gas mixtures, and in particular to the simple experimental approach of observing the flame speed S_s ($=dy_b/dt$) during the pre-pressure period in constant volume bomb explosions with spark ignition at the centre. Here y_b is the radius of the core of burnt gas inside the spherical flame shell, and it is noteworthy that the measurement of dy_b/dt is entirely an objective matter. This situation is in marked contrast with all methods for the direct measurement of burning velocity itself. Strictly, the term burning velocity is only meaningful in relation to planar flame fronts in one-dimensional flow systems, and it is defined as the normal velocity of the unburnt gas relative to the flame front under such conditions. However, whereas theoretical predictions can, and normally do, follow this definition, measured values are obtained from flames which are frequently curved, and in flow systems which are not one-dimensional. It becomes necessary in each case to define a plane which can serve as the reference plane for the flame area in the divergent flow. Without detailed consideration of the flame structure this becomes a subjective matter, as is discussed by Dixon-Lewis and Islam (1982).

Because of the objectivity of their measurement, it seems most logical to use the spherical flame speeds dy_b/dt as the velocity benchmarks for kinetic modelling studies of laminar flames, rather than burning velocities determined by other methods. This is the approach employed in the present paper. It has been used specifically in relation to hydrogen–air flames, for which spherical flame speed measurements at a pressure of one atmosphere, and at a radius of 20 to 30 mm, have been reported by Andews and Bradley (1973). By simulating the spherically expanding flame it has been possible to establish the kinetic model beyond reasonable doubt, and to obtain quantitative agreement with the measured flame speeds for all the mixtures containing more than 20% hydrogen. The model may then be used to compute the normal "planar" burning velocities, and indeed also to investigate possible effects of flame curvature on the rate of movement relative to the unburnt gas. The spherically expanding flame represents a one-dimensional "stretched" flame situation, where there is effectively a shear velocity along the flame front.

Studies of spherically propagating flames are also, of course important in relation to investigations of spark ignition and the prediction of minimum ignition energies (see, for example, Bledjian, 1973; Dixon-Lewis and Shepherd, 1974; Overley *et al.*, 1978; Dixon-Lewis, 1978). Although localized ignition as such is not considered in the present paper, it will be appreciated nevertheless that in spark ignition engines, for example, flame speed may be a more useful characterizing parameter for a combustible mixture than burning velocity.

2 COMPUTATIONAL APPROACH FOR SPHERICAL FLAME PROPAGATION

a) *General Outline*

One of the problems inherent in the study of spherical flames which propagate in the direction of increasing radius, y, is that such flames cannot be maintained stationary against flow perturbations merely by placing a negative material and thermal sink at the centre of the sphere. Theoretical investigation of such flames cannot therefore proceed by an Eulerian approach towards a steady state, and must proceed eventually by a Lagrangian approach governed by the spherical flame equations appropriate to a point ignition of an initially quiescent gas mixture. However, the computational

cost of a Lagrangian calculation from the moment of ignition all the way out to a radius of some 20 or 30 mm, corresponding with the position of experimental determination of the flame speeds, would be excessive. The technique adopted has therefore been, first, to calculate the steady state structure of the planar flame by a forward integration of the time-dependent Cartesian flame equations. This was achieved by use of the "species by species" Eulerian finite difference procedure initially outlined by Spalding, Stephenson and Taylor (1971, 1973), but with incorporation of the detailed transport property formulation as outlined by Dixon-Lewis (1968) and Tsatsaronis (1978). The output from this Eulerian stage of the calculation consists of a steady state "planar" burning velocity together with profiles of all the dependent variables, with the latter finally being expressed in terms of physical distance as the independent variable. These profiles are then used to generate initial profiles for the spherical, Lagrangian flame computation.

In both the planar and the eventual spherical computation, the nodes within the finite difference grid were distributed non-uniformly so that they were at high concentration in the main flame region of high reaction rate and high gradients of the dependent variables, with successively larger spacings between nodes on moving away from this region. The hot boundary of the planar flame became the centre of the spherical grid, and it was arranged that at the end of the planar (and hence start of the spherical) computation the main flame zone was at about 20 mm from this hot boundary. It will be recalled that the planar flame computation has a zero gradient condition for the dependent variables at the truncated hot boundary. This condition automatically provides zero gradients initially at the centre of the sphere. Grids having 50 intervals (53 grid points) were normally used, with some 30 of these intervals being in the main flame zone.

It remains to consider the Lagrangian approach in more detail. The flames will be treated as constant pressure systems, and kinetic energy and viscous effects will be neglected. In the treatment which follows, the composition variables $\sigma_i = w_i/m_i$ will be used, where w_i is the mass fraction of the chemical component i in the volume element under consideration, and m_i is its molecular mass. The σ_i are simply related also to the mole fractions X_i, by

$$\sigma_i = X_i / \sum_i (m_i X_i).$$

There should be no difficulty in distinguishing this use of σ_i, which is confined to Eq. (1) to (20) of the following two sub-sections, from its broader use as a Lennard-Jones (12:6) potential parameter.

b) *Equations to be Solved*

With the assumptions outlined, the Lagrangian forms of the conservation equations governing the one-dimensional, spherically symmetric system become, for a chemical component i:

$$D\sigma_i/Dt = -(1/\rho)\{(1/A)\partial/\partial y(Aj_i/m_i) - R_i\}, \tag{1}$$

and for the specific enthalpy h:

$$Dh/Dt = -(1/\rho)\{(1/A)\partial/\partial y(A[Q_D + Q_T]) - q_E\}. \tag{2}$$

Here ρ is the local mass density, j_i is the diffusive flux of the species i, R_i is its molar rate of formation per unit volume, Q_D and Q_T are enthalpy fluxes due to diffusion

and thermal conduction respectively, q_E is the rate of receipt of energy per unit volume by heat transfer from the surroundings, and A is the area of the spherical shell. Rather than use the complete sphere, it is in practice more convenient to consider a segment subtending a solid angle $(3/4\pi)$ at the centre. In this case the area of the surface becomes $3y^2$.

There is an equation of type (1) for each chemical component in the system. If, as has been done here, a detailed transport flux formulation is used, the transport fluxes in the N-component system are defined (Dixon-Lewis, 1968; Tsatsaronis, 1978) by:

$$j_i = -\{\beta_i^h(\partial h/\partial y) + \sum_{j=1}^{N} \beta_{ij} m_j(\partial\sigma_j/\partial y)\} \tag{3}$$

and

$$q' = Q_D + Q_T$$

$$= -\{\gamma^h(\partial h/\partial y) + \sum_{j=1}^{N} \gamma_j m_j(\partial\sigma_j/\partial y)\}, \tag{4}$$

where:

$$\beta_{ij} = \sum_{k=1}^{N} \{(1-\delta_{ik})\rho\sigma_k D_{ik}(m_i m_k/m_j)\} - (1-\delta_{ij})\rho D_{ij}(m_i/m_G) - \beta_i^h h_j \quad (j = 1,2,\ldots,N \tag{5}$$

$$\beta_i^h = D_i^T/c_p T, \tag{6}$$

$$\gamma_j = \frac{RT}{m_j}\left\{\frac{D_j^T}{m_j\sigma_j} - \sum_{k=1}^{N} \frac{D_k^T m_G}{m_k}\right\} - \frac{\lambda_0 h_j}{c_p} + \sum_{k=1}^{N} h_k\beta_{kj} \quad (j = 1,2,\ldots,N), \tag{7}$$

and

$$\gamma^h = \frac{\lambda_0}{c_p} + \sum_{k=1}^{N} \beta_k^h h_k. \tag{8}$$

Here m_G denotes average molecular mass $[=(\Sigma_j \sigma_j)^{-1}]$, δ_{ij} is the Kronecker delta $(=0$ for $i \neq j$; $=1$ for $i=j)$, T is temperature, c_p is specific heat per unit mass, R is the molar gas constant, the D_{ij} and D_i^T are the multicomponent diffusion coefficients and multicomponent thermal diffusion coefficients respectively, and λ_0 is the thermal conductivity of the mixture. The D_{ij}, D_i^T and λ_0 are computed from the equations of Mason, Monchick *et al.* (1961–1966), as discussed by Dixon-Lewis (1968).

In addition to the conservation equations and the expressions for the transport fluxes, several further relations are required for the closure of the system of equations. These are:

i) A relation between enthalpy and temperature for each chemical species present. These relations were provided here by means of second order polynomial fits of thermal data over 300° temperature ranges. We then have:

$$h = \sum_i (\sigma_i H_i)$$

$$= \sum_i \sigma_i (a_0 + a_1 T + a_2 T^2), \tag{9}$$

where H_i is the molar enthalpy, and a_0, a_1 and a_2 are polynomial coefficients.

ii) The ideal gas equation of state:

$$P/\rho = \left(\sum_i \sigma_i\right) RT \tag{10}$$

iii) Rather than set up a species conservation equation for each of the N components of the reacting system, the physical nature of the problem was preserved against possible numerical rounding errors by replacing the equation for N_2 in the present system by:

$$\sigma_{N_2} = \left(1 - \sum_{i \neq N_2} m_i \sigma_i\right) / m_{N_2}. \tag{11}$$

Equation (11) simply expresses the condition that the sum of the mass fractions of all the components must always be unity.

iv) Lastly, the chemical rates R_i must be defined. For the elementary chemical reaction:

$$A + B \underset{k_{-1}}{\overset{k_1}{\rightleftharpoons}} C + D$$

the net molar forward rate is given by:

$$R = k_1 \rho^2 (\sigma_A \sigma_B - \sigma_C \sigma_D / K_1), \tag{12}$$

where k_1 is the forward reaction rate coefficient, and K_1 is the equilibrium constant of the reaction ($=k_1/k_{-1}$). Both the rate coefficients, and the equilibrium constant, are functions of temperature, being expressed by way of the Arrhenius type equation:

$$k = A T^B \exp(-C/T), \tag{13}$$

or the van't Hoff isochore:

$$K = D T^E \exp(-F/T). \tag{14}$$

The rate of formation of each species i in a chain reaction is obtained by summation over the elementary steps.

The complete set of equations must then be solved subject to the boundary conditions (for the spherical flame):

$$\left.\begin{array}{llll} y = 0; & \partial\sigma_i/\partial y = 0, & \partial h/\partial y = 0 & \\ y = \infty; & \sigma_i = \sigma_{iu}, & h = h_u(T_u, \sigma_{iu}), & \\ & \partial\sigma_i/\partial y = 0, & \partial h/\partial y = 0 & \end{array}\right\} \tag{15}$$

The objective of the Lagrangian calculation is to observe the evolution of the flame profiles with time.

c) *Solution of Equations*

As the first step towards a solution, Eqs. (1) and (2) are transformed into the von Mises system of co-ordinates. For the Lagrangian formulation the transformation is defined simply by:

$$d\psi/dy = \rho A, \tag{16}$$

since in the absence of a convective term the value of the stream function ψ associated with any fluid element remains constant with time. Proceeding along the same lines as Spalding and Stephenson (1971), Spalding *et al.* (1971), and Stephenson and Taylor (1973), and introducing a dimensionless stream function ω defined by:

$$\omega = \frac{\psi - \psi_b}{\psi_u - \psi_b} \quad (0 < \omega < 1), \tag{17}$$

the difference $(\psi_u - \psi_b)$ defines a finite total mass of fluid within the computational domain. In the planar flame calculation the finite mass corresponds with a stream tube area which is everywhere unity. The process indicated in Section 2(a), of translation of the steady state planar flame profiles into starting profiles for the Lagrangian calculation in spherical von Mises co-ordinates, thus involves appropriate adjustments of the stream functions ψ and ω to take account of the spherical geometry. In the spherical case $\psi_b = 0$, and ψ_u represents the total mass of fluid in the finite spherical domain. In spherical von Mises co-ordinates, Eqs. (1) and (2) become:

$$D\sigma_i/Dt = -(1/\psi_u)\partial/\partial\omega(Aj_i/m_i) + R_i/\rho \tag{18}$$

$$Dh/Dt = -(1/\psi_u)\partial/\partial\omega\{A(Q_D + Q_T)\} + q_E/\rho \tag{19}$$

with the boundary conditions:

$$\left.\begin{aligned} &\omega = 0, 1; \quad \partial\sigma_i/\partial\omega = 0, \qquad \partial h/\partial\omega = 0 \\ &\omega = 1; \qquad \sigma_i \quad = \sigma_{iu}, \quad h \quad = h_u(T_u, \sigma_{iu}) \end{aligned}\right\} \tag{20}$$

We note that, if the vector of the dependent variables is denoted by $\mathbf{\Phi}$, Eqs. (18) and (19) to be integrated may be written as the matrix equation:

$$D\mathbf{\Phi}/Dt = -(1/\psi_u)\partial/\partial\omega(A\mathbf{Q}) + \mathbf{d} \tag{21}$$

where $(A\mathbf{Q})$ represents the transport flux terms in Eqs. (18) and (19), and $\mathbf{d}$ represents the terms R_i/ρ or q_E/ρ which do not contain ω. By reference to Eqs. (3) to (8), it can be seen that the terms of $\mathbf{Q}$ take the form:

$$Q_i = -\sum_{k=1}^{N+1} \beta_{ik}'(\partial\phi_k/\partial y) \quad (i = 1, 2, \ldots, N+1), \tag{22}$$

where the first N integers i and k refer to the chemical components, and the $(N+1)$th integer refers to the specific enthalpy.

The finite difference calculations in the (ω, t)-plane were carried out by a fully implicit method, and the conversion of the differential to finite difference equations employed the technique described by Patankar and Spalding (1970) of micro-integration with respect to ω across each finite difference cell. The procedure assumes a linear variation of all properties with ω between successive nodes, and the cell boundaries

between the nodes were arranged so as to divide each inter-nodal interval $\delta\omega$ into equal parts each of magnitude $\delta\omega/2$. To the set of non-linear algebraic equations resulting from the finite differencing must then be added the auxiliary relations (9) and (10) which define the temperature and density, and additionally, relationships which define the half-cell volumes and the physical distances between each cell centre and its boundaries. The former are required explicitly for the calculation of the space integral rates

$$\int_0^{\partial\omega/2} (R_i/\rho)d\omega,$$

and are obtained by dividing the mass increments $\delta\omega/2$ by the appropriate average density for the half-cell. Successive summation of the volumes from the centre outwards then also gives the spherical segment volumes from the centre out to each cell boundary and nodal plane, from which in turn the appropriate internodal distances and cell boundary areas may be calculated. Both are required for the computation of the diffusive fluxes. The overall procedure will be described in greater detail elsewhere (Dixon-Lewis, 1983). For the spherically propagating flame it results in a total of $(N+5)$ algebraic equations to be solved simultaneously at each grid point, with diffusive coupling between grid points leading to the familiar tridiagonal matrix form for the equations over the whole grid. Adopting a Newton–Raphson iterative approach with linearization of each of the dependent variables about an estimated solution, the resulting set of linear equations was solved to obtain the Newton–Raphson corrections by a standard combination (Richtmyer and Morton, 1967; Roache, 1972) of Gaussian elimination with a forward and a backward pass successively through the grid so as to remove the diffusive coupling at each side of each intermediate interval, and eventual solution of the $(N+5)$ equations in $(N+5)$ unknowns at each grid point. Iteration was repeated until satisfactory convergence was achieved over the whole grid. This completes the main cycle of computation at each time step. Time intervals of between 10^{-7} and 10^{-6} s were employed, depending on the flame.

After a large number of cycles of computation in the manner outlined, it was found that accumulation of errors caused the computed densities to depart very slightly from the "check" values computed from the new compositions and temperatures. These departures are believed to be due to the first order nature of the calculation, and they are common to both planar and spherical Lagrangian computations. Since the densities also determine the volumes of the half-cells, it was decided further to correct both the temperatures and densities at the end of each time step, so as to conform precisely with the compositions and enthalpies at each grid point. The corrected values were obtained by direct application of Eqs. (9) and (10).

d) *Boundary Conditions*

The sub-division of the computational grid as outlined above leaves a half-interval at each end. These half-intervals are used to incorporate the boundary conditions. They are coupled diffusively into the grid at only one boundary, and it is this feature which permits commencement of the forward and backward Gaussian elimination sweeps. In the present context it was arranged that the central spherical half-interval had uniform properties across it, with its diffusive coupling depending on the gradients of the dependent variables across the *half*-interval next furthest out. Normally the

total distance over *two* half-intervals is used for this purpose. At the outermost half-interval of the grid the dependent variables are defined directly by the cold boundary conditions of the flame at $\omega=1$.

e) *Regridding*

Because of the outward movement of the flame in the spherical co-ordinate system, it was necessary, in order to retain computational precision within the main flame zone, that the closely spaced region of the grid should be advanced more or less along with the flame. The grid nodes in the closely spaced region were numbered from 11 to 43, with the node density rapidly becoming smaller on moving away from this region through the nine intervals $\delta\psi$ (or $\delta\omega$) towards either the centre or the outside of the sphere. The regridding procedure was brought into operation between computational time steps on each occasion when the flame had advanced through one of the $\delta\psi$ intervals of the closely spaced region. The grid was advanced so that the nodes numbered 12 to 43 at the start became the "new" nodes 11 to 42. The extra interval between the old nodes 11 and 12 was then absorbed into the central, more widely spaced region simply by increasing the stream function ψ at each of the old nodes 0 to 10 in the ratio $(\psi_{12}/\psi_{11})_{\text{old}}$, whilst at the same time interpolating linearly on the old values of the dependent variables so as to conform with the new ψ in the central region. Small and consistent corrections were then made to the positions of interpolation (though not to the new stream functions), so that after recalculation of the temperatures, densities and half-cell volumes in the central region, the total spherical volume out to the "new" node 11 was the same as that out to the "old" node 12. The procedure preserves the physical situation intact in the important reaction region of the flame.

A similar procedure was followed at the outer boundary of the sphere, where it was necessary to insert an extra node. The stream functions belonging to the "old" nodes 43 to 53 were simply increased in the ratio $(\psi_{43}/\psi_{42})_{\text{old}}$ to give the values at the new nodes. The dependent variables were adjusted in the same manner as at the centre of the sphere. The regridding process thus also increases the total mass of fluid within the grid, and allows in an economical manner for the outward radial movement of the flame.

f) *Determination of Flame Speeds, Gas Velocities and Burning Velocities in Spherical Propagation*

The primary output from the Lagrangian computation at the end of any time step consists of tables of composition variables, enthalpies, temperatures, densities and radial distances. Radial profiles of the dependent variables may be constructed from these. The velocity of radial advance of the temperature profile was chosen for the determination of the flame speed (though any other profile would serve just as well). Temperatures and distances at the grid nodes were printed to eight and nine significant decimal digits respectively, at intervals of 200 time steps. Four or five temperatures, evenly distributed in the main flame zone (usually at points 15, 22, 29, 36 and 41 of the initial grid), were then chosen, and the radial distances corresponding with these temperatures were calculated at later times by linear interpolation in the appropriate output. The flames were normally observed to settle to a steady velocity after about 5 to 7 mm of travel, the steady velocity being the sought-after flame speed, S_s.

By way of explanation, the necessity for definition of the temperatures and distances

to this very high degree of precision arises from the large difference between the distance scale of the flame radius on the one hand, and its movement during a time interval of the order of 10^{-7} to 10^{-6} s on the other. It is on the distances of movement that attention is focused directly during the computation.

Because the gas consumed by the spherical flame expands as it burns, the central core of burnt gas pushes the unburnt gas radially outwards ahead of it. The gas velocities V_g at the grid nodes may be obtained at any instant from the radial distance increments during a single time step. Gas velocities at intermediate points, for example at the four or five reference temperatures above, may again be obtained by linear interpolation. Provision for determining the gas velocities in this way was made in conjunction with the periodic outputs above. It then becomes possible to observe the velocity $(S_s - V_g)$ of the curved flame relative to the gas supporting it, and thus, after multiplication by the density ratio ρ/ρ_u, to determine a spherical flame analogue of the linear burning velocity of the planar flame. Here ρ is the density of the gas with velocity V_g. For steady propagation, such "spherical burning velocities" will be more or less independent of the positions of the reference planes (or temperatures) at which they are determined.

3 REACTION RATE AND TRANSPORT PARAMETERS APPROPRIATE TO THE HYDROGEN-OXYGEN-NITROGEN FLAME SYSTEM

a) *Introductory Remarks*

The kinetic modelling of the hydrogen–oxygen–nitrogen flame has previously been discussed in some detail by Dixon-Lewis (1979), and the more important reactions controlling the flame velocity have been shown to be:

$$\begin{aligned}
OH + H_2 &\rightleftharpoons H_2O + H && \text{(i)}\\
H + O_2 &\rightleftharpoons OH + O && \text{(ii)}\\
O + H_2 &\rightleftharpoons OH + H && \text{(iii)}\\
H + O_2 + M &\rightleftharpoons HO_2 + M && \text{(iv)}\\
H + HO_2 &\rightleftharpoons OH + OH && \text{(vii)}\\
H + HO_2 &\rightleftharpoons O + H_2O && \text{(viia)}\\
H + HO_2 &\rightleftharpoons H_2 + O_2 && \text{(xii)}\\
OH + HO_2 &\rightleftharpoons H_2O + O_2 && \text{(xiii)}\\
O + HO_2 &\rightleftharpoons OH + O_2 && \text{(xiv)}\\
H + H + M &\rightleftharpoons H_2 + M && \text{(xv)}\\
H + OH + M &\rightleftharpoons H_2O + M && \text{(xvi)}\\
H + O + M &\rightleftharpoons OH + M && \text{(xvii)}\\
OH + OH &\rightleftharpoons O + H_2O && \text{(xviii)}
\end{aligned}$$

However, the rate parameters associated with many of these elementary reaction steps are still only imperfectly known; and although predictions of the burning velocities of the whole flammable range of hydrogen–air mixtures at atmospheric pressure have been made by both Warnatz (1978, 1981) and Dixon-Lewis (1979), *a priori* allowable differences between their assumed reaction rate and diffusion parameters led to very appreciable differences between the predicted values. Thus, for the 41 percent hydrogen–air flame by volume at atmospheric pressure, the respective predictions were 330 and 267 cm s^{-1}. Dixon-Lewis used both a lower diffusion coefficient for hydrogen atoms and a lower reaction rate coefficient k_2 than did Warnatz, and his

sensitivity analysis (Dixon-Lewis, 1979) showed that an increase in either of these coefficients would increase the predicted burning velocity for the specific flame. The difficulty of definition of the rate parameters really lies with the subjectivity of the burning velocity measurements with which the predictions are normally compared. As already discussed, the flame speed of the spherically expanding flame provides a more objective measurement for comparison, and the remaining task in the case of the hydrogen–oxygen–nitrogen system is therefore to establish a set of reaction rate and diffusion parameters which satisfactorily predict the observed flame speeds. The initial investigation, described in the present section, is again performed with reference to the properties of the 41 percent hydrogen–air flame at atmospheric pressure, for which Andrews and Bradley (1973) measured a "spherical" flame speed of 1750 cm s^{-1} at a radius of 25 mm. After an examination in Section 4 of the consistency of the newly derived data with measured radical decay profiles in fuel-lean flames, and with lower temperature hydrogen–oxygen–nitrogen flame properties, these new data are used in Section 5 for the prediction of both flame speeds and normal burning velocities for the whole flammable range of hydrogen–air mixtures.

b) *Review of Background Kinetic Information*

As a preliminary to the discussion of the spherically expanding 41 percent hydrogen–air flame, it will be convenient to review, and occasionally update, some of the background kinetic information. Thus:

i) All the equilibrium constants, and the rate parameters for reactions (i), (iii), (xv), (xvi), (xvii) and (xviii) remain as used by Dixon-Lewis (1979). These values are given in Table IV.

ii) The ratios k_2/k_4 at temperatures around 773 K are reliably known from second explosion limit measurements in the hydrogen–oxygen system. In this paper an activation energy of 70.3 kJ mol^{-1} is also assigned to reaction (ii).

iii) Near room temperature, Bishop and Dorfman (1970) found $k_{4,H_2}=(17\pm4)\times 10^{15}$ cm^6 mol^{-2} s^{-1} at 298 K, while Wong and Davis (1974) obtained $k_{4,H_2}=(21.7\pm 4.3)\times 10^{15}$ and Moortgat and Allen (1972) found $k_{4,H_2}=23.2\times 10^{15}$. All these results are in good agreement with each other, and clearly then, the expression chosen for k_4 must be consistent with them.

iv) Subsequently to the earlier computations by Dixon-Lewis (1979), there have been measurements by Hack *et al.* (1978, 1979) of all the rate coefficients k_7, k_{7a}, k_{12}, k_{13} and k_{14} at or near room temperature. The mean measured values of k_{13} and k_{14} have been incorporated into Table IV, with the assumptions that both reactions have zero activation energy. The older values used by Dixon-Lewis (1979) are given in parentheses in the Table.

v) As previously, the important ratio $(k_7+k_{7a})/k_{12}$ was assigned a value close to 6.0 at 773 K, in agreement with the analysis of Baldwin *et al.* (1974) of their hydrogen–oxygen second explosion limit data in boric acid coated vessels. For $(k_7+k_{7a})/k_{12}=5.95$ at 773 K (the value actually assigned in all except one or two of the sensitivity investigations described below), the results of Baldwin *et al.* also led to $(k_7+k_{7a})^2/k_2^2k_{10}=3.25\times 10^{-4}$ mol cm^{-3} s, and in turn, for an estimated $k_{10}=2.0\times 10^{12}$ at 773 K (see Dixon-Lewis and Williams, 1977; Dixon-Lewis, 1979), to the set of ratios of rate coefficients given in Table I. Reaction (x) is:

$$HO_2 + HO_2 = H_2O_2 + O_2 \qquad (x)$$

TABLE I
Ratios of rate coefficients at 773K. (Units, where applicable, are appropriate cm mol s units)

$(k_7+k_{7a})/k_{12}$	5.95
$(k_7+k_{7a})^2/k_2^2k_{10}$	3.25×10^{-4}
$(k_7+k_{7a})/k_2$	2.55×10^{4}
$k_2/k_{4,H_2}$	3.84×10^{-7}
k_{12}/k_2	4.30×10^{3}

vi) The discharge–flow measurements of Hack, Wagner and Hoyermann (1978) on the reaction of hydrogen atoms with hydroperoxyl led to values of k_7, k_{7a} and k_{12} at 293 K, and to a ratio $(k_7+k_{7a})/k_{12}=2.4$ at this temperature. The quoted ratio is in exact agreement with the median result of Clyne and Thrush (1963), who used a less precise technique for its measurement at the same temperature; and it has been adopted here as a fixed low temperature value. In combination with the value of 5.95 at 773 K it leads to the Arrhenius expression $(k_7+k_{7a})/k_{12}=10.4\exp(-430/T)$. The non-parenthesized parameters in Table IV conform with this expression, and with the absolute values of k_7 and k_{12} found by Hack *et al.* The value used earlier by Dixon-Lewis (1979) for the ratio $(k_7+k_{7a})/k_{12}$ is given in parentheses at the bottom of the Table.

The important unknown kinetic parameters at 773 K have now all been expressed in terms of k_2 (see Table I); and since an activation energy has also been assigned to reaction (ii), then the constraints and assumptions outlined are such that the *reaction kinetics* of the system is completely defined once the pre-exponential factor A_2 is established.

c) *Transport Parameters*

Molecular interactions for the transport property calculations were represented by the Lennard-Jones (12:6) potential, with the use of the force constants given in Table II. Except for σ_H these are all values recommended by Svehla (1962). The value of σ_H will be discussed below.

TABLE II
Lennard-Jones (12:6) potential parameters

Species	(eps/k)/K	σ/nm	ζ_{tj} (collisions)
H	37.0	0.2250	—
		(0.35, 0.30)	
O	106.7	0.3050	—
OH	79.8	0.3147	4.5
N_2	71.4	0.3798	4.5
O_2	106.7	0.3467	4.5
H_2	59.7	0.2827	200.0
H_2O	260.0	0.2800	4.0
HO_2	168.0	0.3068	—

Most of the remaining data for the transport property calculations have been given by Dixon-Lewis (1968). Because H_2O is the polar component present in major concentration in all the mixtures studied, and because the theory will deal only with mixtures containing not more than one polar component, all other species were considered to be non-polar.

The collision numbers ζ_{ij} assumed for rotational relaxation of each polyatomic species i on colliding with any other species j are given in the fourth column of Table II. These are required only for the thermal conductivity and thermal diffusion calculation, from which HO_2 is omitted.

The values of σ_H require further comment. Firstly, on account of their small molecular mass, hydrogen atoms are the principal contributors to the diffusion of radicals in the flames. Secondly, Clifford *et al.* (1982) have recently measured the diffusion coefficients of hydrogen atoms in both nitrogen and argon, and find $\mathscr{D}_{H,N_2} = 1.35 \pm 0.03$ and $\mathscr{D}_{H,Ar} = 1.61 \pm 0.04$ cm^2 s^{-1} respectively at 294 K and atmospheric pressure. Taking the former value in combination with σ_{N_2}, $(eps)_H/k$ and $(eps)_{N_2}/k$ from Table II (and incidentally, thereby implying a specific temperature dependence of the diffusion coefficient) leads, by the standard expression for a binary diffusion coefficient, to $\sigma_H = 0.207$ nm. The non-parenthesized value given in Table II is 0.225 nm. The values of σ_H given *in* parentheses are values which were used by Dixon-Lewis (1979). In combination with the set of reaction rate parameters used at that time they led to predicted burning velocities of 254 and 265 cm s^{-1} for the 41 percent hydrogen–air flame (for $\sigma_H = 0.35$ and 0.30 nm respectively). In view of the sensitivity analysis (Dixon-Lewis, 1979) already referred to in Section 3(a), the implication of the new measurement and the new value of σ_H is clear.

d) *Predictions of Planar Burning Velocity and Spherical Flame Speed of 41 percent Hydrogen–Air Flame. Preliminary Optimization of Adjustable Parameters*

Exploratory investigations were carried out on the flame having the initial mole fraction composition $X_{H_2,u} = 0.4100$, $X_{O_2,u} = 0.1239$ and $X_{N_2,u} = 0.4661$, with $T_u = 298$ K, at atmospheric pressure. The results of a number of trial runs with different values of the several adjustable parameters are given in Table III as predictions of the "planar" burning velocity S_u and, where calculated, the "spherical" flame speed S_s at a radius of 25 mm.

TABLE III

Predictions of planar burning velocity and spherical flame speed for mixture having initial mole fraction composition $X_{H_2,u} = 0.4100$, $X_{O_2,u} = 0.1239$ and $X_{N_2,u} = 0.4661$, with $T_u = 298$ K, at atmospheric pressure

Run	$\frac{k_7 + k_{7a}}{k_{12}}$	k_{4,H_2} at 298 K,[a] 10^{16} cm^6 mol^{-2} s^{-1}	σ_H, nm	A_2, 10^{14} cm^3 mol^{-1} s^{-1}	S_u, cm s^{-1}	S_s, cm s^{-1}
1	12.0 exp(−540/T)	1.7	0.300	1.7	263	*ca.* 1550
2	12.0 exp(−540/T)	1.7	0.300	2.2	290	—
3	12.0 exp(−540/T)	1.7	0.250	2.2	310.5	—
4	12.0 exp(−540/T)	1.7	0.225	2.2	322.0	—
5H	12.0 exp(−540/T)	1.7	0.225	2.2	319.4	—
6H	9.57 exp(−425/T)	1.7	0.225	2.2	319.5	—
7H	6.68 exp(−300/T)	1.7	0.225	2.2	315.3	—
8H	6.68 exp(−300/T)	2.0	0.225	2.2	314.6	—
9H	9.26 exp(−390/T)	2.0	0.225	2.2	319.8	—
10H	9.26 exp(−390/T)	2.0	0.225	2.1	312.4	*ca.* 1830
10HR						*ca.* 1830
11H	10.4 exp(−430/T)	2.0	0.225	1.8	296.5	—
12H	10.4 exp(−430/T)	2.0	0.225	1.9	300.0	1778

[a] In combination with k_{4,H_2} at 773 K, this data point defines the temperature dependence of k_4.

Several important features emerge:

i) The conditions of run 1 correspond closely with the transport and rate parameters used earlier by Dixon-Lewis (1979). They predict a spherical flame speed of only about 1550 cm s^{-1}, compared with the measured value of 1750 cm s^{-1}. If, as is commonly assumed, the measured flame speed is low by about 5 percent on account of radiative and other cooling losses, then an adiabatic flame speed prediction of around 1835 cm s^{-1} and a burning velocity prediction near 310 cm s^{-1} should be sought for the 41 per cent hydrogen–air flame.

ii) With A_2 retained constant throughout at 2.2×10^{14} cm^3 mol^{-1} s^{-1}, thus preserving the expression for k_2 recommended by Baulch *et al.* (1972), runs 2 to 9H examine the sensitivity of the planar burning velocity, firstly, to changes in σ_H, secondly, to trial values of k_{13} and k_{14}, thirdly, to moderate reductions (down to a minimum of 4.5) in the ratio $(k_7+k_{7a})/k_{12}$ at 773 K, and fourthly, to admissible changes in the value of k_{4,H_2} at 298 K. The purely numerical run identifications denote continued use of the earlier values of k_{13} and k_{14} estimated by Dixon-Lewis (1979). The identifications terminating in "H" denote use of the values found by Hack *et al.* (1978, 1979) at room

TABLE IV

Parameters of expressions for forward rate coefficients and independent equilibrium constants in hydrogen–oxygen–nitrogen flame mechanism. Rate coefficients are expressed as $k=AT^B\exp(-C/T)$ and equilibrium constants as $K=DT^E\exp(-F/T)=k_{forward}/k_{reverse}$, both in appropriate cm mol s units

	Reaction	A	B	C/K	D	E	F/K
(i)	$OH+H_2 \rightleftharpoons H_2O+H$	1.17×10^{9}	1.3	1825	0.21	0	−7640
(ii)	$H+O_2 \rightleftharpoons OH+O$	1.9×10^{14}	0	8450	300.0	−0.372	8565
(iii)	$O+H_2 \rightleftharpoons OH+H$	1.8×10^{10}	1.0	4480	2.27	0	938
(iv)[a]	$H+O_2+H_2 \rightleftharpoons HO_2+H_2$	2.7×10^{18}	−0.86	0	0.745	0	−23380
(vii)	$H+HO_2 \rightleftharpoons OH+OH$	2.1×10^{14}	0	710			
		$(1.4\times10^{14}$	0	540)			
(viia)	$H+HO_2 \rightleftharpoons O+H_2O$	1.05×10^{13}	0	710			
		$(1.0\times10^{13}$	0	540)			
(xii)	$H+HO_2 \rightleftharpoons H_2+O_2$	2.12×10^{13}	0	280			
		$(1.25\times10^{13}$	0	0)			
(xiii)	$OH+HO_2 \rightleftharpoons H_2O+O_2$	1.8×10^{13}	0	0			
		$(7.5\times10^{12}$	0	0)			
(xiv)	$O+HO_2 \rightleftharpoons OH+O_2$	2.0×10^{13}	0	0			
		1.4×10^{13}	0	540 a	$\rightarrow k_{14}=k_{14a}+k_{14b}$		
		1.25×10^{12}	0	0 b			
(xv)	$H+H+H_2 \rightleftharpoons H_2+H_2$	9.2×10^{16}	−0.6	0	0.24	0	−52590
	$H+H+N_2 \rightleftharpoons H_2+N_2$	1.0×10^{18}	−1.0	0			
	$H+H+O_2 \rightleftharpoons H_2+O_2$	1.0×10^{18}	−1.0	0			
	$H+H+H_2O \rightleftharpoons H_2+H_2O$	6.0×10^{19}	−1.25	0			
(xvi)	$H+OH+M \rightleftharpoons H_2O+M$						
	$M=H_2, O_2, N_2$	1.6×10^{22}	−2.0	0			
	$M=H_2O$	8.0×10^{22}	−2.0	0			
(xvii)	$H+O+M \rightleftharpoons OH+M$						
	$M=H_2, O_2, N_2$	6.2×10^{16}	−0.6	0			
	$M=H_2O$	3.1×10^{17}	−0.6	0			
(xviii)	$OH+OH \rightleftharpoons O+H_2O$	5.75×10^{12}	0	390			
Ratio	$(k_7+k_{7a})/k_{12}$	10.4	0	430			
		(12.0	0	540)			

[a]Chaperon efficiencies relative to $H_2=1.0$ are 0.44, 0.35 and 6.5 for N_2, O_2 and H_2O respectively.

temperature. Additionally, the runs 7H to 12H all have $(k_7=k_{7a})/k_{12}=2.4$ at 293 K; and runs 1 to 5H, 11H and 12H all have $(k_7+k_{7a})/k_{12}=5.95$ at 773 K.

These particular sensitivity tests show that with A_2 retained constant only the changes in σ_H appreciably influence the prediction of the 41 percent hydrogen–air flame velocity.

iii) With σ_H constant at 0.225 nm, runs 9H to 12H show the effect of reductions in the pre-exponential factor A_2 on the predicted planar burning velocity. Runs 10H and 10HR are of further interest since they examine the sensitivity of the spherical flame speed prediction to radiative loss of heat from the core of burnt gas. Run 10H refers to an *adiabatic* spherically expanding flame, that is, the heat exchange term q_E in Eqs. (2) and (19) was set equal to zero. Run 10HR included an estimated radiative heat loss by means of the term:

$$q_E = -4.32 \times 10^{-8}\, T^4 \quad \text{J m}^{-3}\,\text{s}^{-1}, \tag{23}$$

which would correspond with an average burnt gas emissivity over the whole spectrum of just over 0.006. Inclusion of this radiative loss term made a barely perceptible difference to the double precision result of the flame speed computation, and it was decided therefore that the 5 percent allowance for cooling losses was unrealistic. An adiabatic flame speed near 1750 cm s^{-1} was thus subsequently sought. Run 12H gives a satisfactory result. The reaction rate parameters leading to this prediction are given as the non-parenthesized parameters in Table IV. They lead to a planar burning velocity of 300 cm s^{-1}.

4 FURTHER CONSIDERATION OF RATE PARAMETERS

A brief examination of Table III shows that the set of rate parameters given in Table IV is not unique in satisfying the flame speed requirement. A whole spectrum of other combinations of A_2 and σ_H may also lead to the observed spherical flame speed of near 1750 cm s^{-1} for the 41 percent hydrogen–air mixture. The selection of an appropriate single combination of these parameters necessitates consideration of other properties of the hydrogen–oxygen–nitrogen flame system. Such an examination is the purpose of the present section.

a) *Radical Recombination in High Temperature, Fuel-Lean Flames*

Friswell and Sutton (1972) used the lithium/lithium hydroxide method to measure hydrogen atom profiles in the burnt gas regions of four fuel-lean hydrogen–oxygen–nitrogen flames at atmospheric pressure, at temperatures in the region of 2100 K. The properties of the four flames, together with the approximate percentages of recombination by the possible routes, are given in Table V, and the profiles of $[H]^{-1}$ are shown in Figure 1. The points in Figure 1 refer to the observations of Friswell and Sutton (1972), while the solid lines have been computed on the basis of partial equilibrium assumptions on reactions (i), (ii), (iii) and (xviii). The calculation followed in detail the composite flux method described by Dixon-Lewis *et al.* (1975), and the reaction rate and equilibrium parameters were taken from Table IV. The transport parameters were those of Table II. Agreement with experiment is good. The right-hand columns of Table V clearly show the importance of recombination by the HO_2 route, and although k_2 does not enter *directly* into the computation, it does exert a

powerful indirect influence by virtue of its position in all the ratios $(k_7+k_{7a})/k_2$, $k_2/k_{4,H_2}$ and k_{12}/k_2 at 773 K (Table I). The closely defined room temperature values of k_{4,H_2}, k_7, k_{7a} and k_{12} are fixed independently of k_2, so that at 2100 K the dependence on k_2 enters by way of the Arrhenius type expressions for the rate parameters. The expression $k_{4,H_2}=2.7\times10^{18}\,T^{-0.86}$ cm^6 mol^{-2} s^{-1} given in Table IV leads to $k_{4,H_2}=$

TABLE V

Properties of high temperature, fuel-lean hydrogen-oxygen-nitrogen flames in recombination region.

[Flames are those for which H atoms concentrations are given by Friswell and Sutton (1972)]

Flame	p/atm	$(H_2/O_2)_u$	$(N_2/O_2)_u$	V_b/cm s^{-1}[a]	Approx. temp. range of recombination °K	Approx. % recombination at ends of range of measurement by (xv) H+H+M	(xvi) H+OH+M	(iv) H+O$_2$+M
A	1.0	1.67	4.00	1130	1850–2125	4.7–0.7	27–28	66–70
B	1.0	1.54	3.61	1130	1840–2140	3.7–0.4	24–22	71–77
C	1.0	1.43	3.29	1130	1800–2135	3.5–0.3	21–19	74–81
D	1.0	1.33	3.00	1130	1850–2135	2.0–0.2	18–16	80–83

[a] V_b gives linear burnt gas velocity at standard condition of 2000 K and p atm pressure.

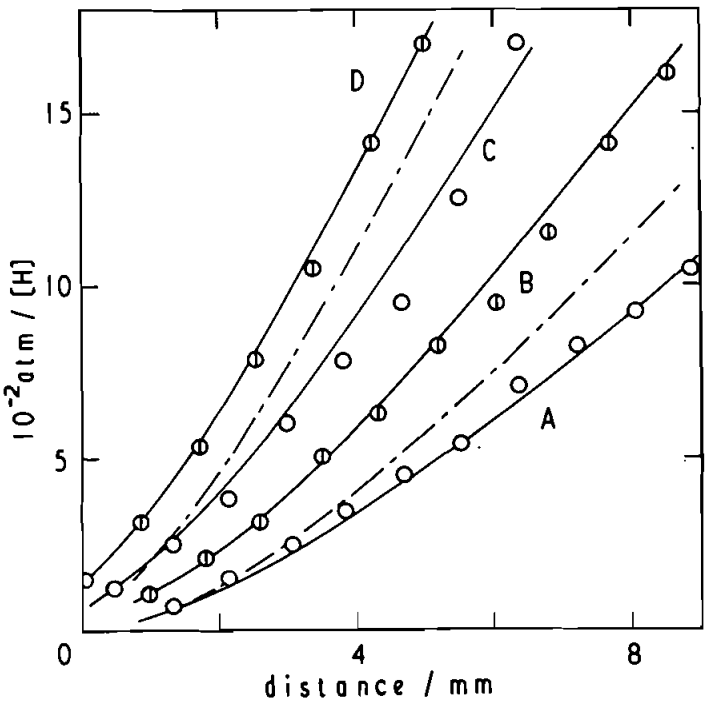

FIGURE 1 Recombination in fuel-lean hydrogen–oxygen–nitrogen flames. Comparison of measured points of Friswell and Sutton (1972) with computed lines. Letters refer to flames of Table V. Solid lines refer to transport and reaction rate parameters from Tables II and IV. Dot/dashed lines for flames A and C: reaction rate coefficients calculated from Table I on basis of $A_2=2.2\times10^{14}$ cm^3 mol^{-1} s^{-1}.

2.0×10^{16} and 3.9×10^{15} at 298 and 2000 K respectively. The former value is well within the experimental error ranges quoted by both Bishop and Dorfman (1970), and Wong and Davis (1974).

To illustrate the effect of changes in A_2 on the profiles of Figure 1, further computations were performed for flames A and C of Table V, with the rate coefficients k_{4,H_2}, k_7, k_{7a} and k_{12} at 773 K calculated from Table I on the basis of $k_2=2.2\times10^{14}$ $\exp(-8450/T)$ cm^3 mol^{-1} s^{-1}. The dot/dashed lines in the figure show the new profiles. The predicted recombination rate is clearly too high. As a preliminary to discussion, it should be noted that diffusion effects will be small in the fast-moving burnt gases of these flames. The observed profiles are thus almost entirely kinetically controlled. Next, the rate of the major recombination process via the HO_2 route depends, firstly, on the rate of primary formation of HO_2 by reaction (iv), and secondly, on the competition of the *summed* effects of ractions (vii), (viia), (xii), (xiii) and (xiv) with the re-dissociation reaction (-iv). The major contributors to the summed effect are the reactions (vii), and, retaining (k_7+k_{7a}) constant, reasonable changes in the ratio $(k_7+k_{7a})/k_{12}$, say down to 4.5, will give only small consequential changes in the summed recombination rate. The computed profiles thus ultimately depend, for a given k_2, on the second explosion limit analysis of Baldwin *et al.* (1974) to give the ratio $R=(k_7+k_{7a})^2/k_2^2\,k_{10}$, and on the assumption regarding k_{10} at 773 K [see Section 3(b)]. The ratio R increases with decreasing $(k_7+k_{7a})/k_{12}$ (Baldwin *et al.*, 1974), and the increased A_2 in the revised runs would, if anything, be accompanied by just such a decrease (see Table III, runs 8H and 9H). Unless k_{10} is considerably less at 773 K than at room temperature, it is therefore most uhlikely that the ratio $(k_7+k_{7a})/k_2$ in Table I is an over-estimate. Consideration of the high temperature recombination together with the results at room temperature and at 773 K thus very strongly suggests that $A_2=2.2\times10^{14}$ is too high, and that the optimum value of A_2 is near 1.9×10^{14} cm^3 mol^{-1} s^{-1}.

b) *Radical Recombination in Fuel-lean Flames at Lower Temperatures (Up to 1500 K)*

In this section three fuel-rich and four fuel-lean flames are studied, for which profiles of the decay of hydroxyl radical concentration in the recombination regions were

TABLE VI

Properties of several hydrogen–oxygen–nitrogen flames in the recombination region. |Flames are those for which OH concentrations were measured by Kaskan (1958a, b), and re-calibrated as discussed by Dixon-Lewis (1979)|

Flame	p/atm	$(H_2/O_2)_u$	$(N_2/O_2)_u$	V_b/(cm s^{-1})[a]	Approx. temp. range of recombination °K	Approx. % primary recombination at ends of range by (xv) H+H+M	(xvi) H+OH+M	(iv) H+O$_2$+M
E	1.0	2.05	3.76	27.5	1550–1685	8– 7	36–80	55–13
F	0.5	3.48	3.76	51.0	1230–1310	95–87	5–12	v. small
G	0.5	2.38	3.76	35.3	1400–1540	47–47	38–52	14– 2
H	0.45	1.00	3.76	18.8	1330–1410	v. small	4.1–0.4	95.4–99.6
I	0.45	1.60	3.76	11.9	1370–1430	v. small	7.2–1.2	92.2–98.8
J	1.0	1.00	3.76	33.4	1520–1530	v. small	2.0–0.5	97.9–99.5
K	1.0	1.60	3.76	16.8	1500–1530	v. small	6.7–1.5	93.0–98.5

[a] V_b gives linear burnt gas velocity corrected to standard conditions of 298 K and p atm pressure.

measured by Kaskan (1958a, b). These concentrations were measured by ultra-violet absorption spectroscopy, and as a result of a private communication from the late Professor Kaskan in 1974, which resolved several uncertainties associated with the original calibration, this original calibration was revised by Dixon-Lewis (1979). The recalibrated profiles of $[OH]^{-1}$ are shown as the points in Figures 2 to 4, for the flames with properties given in Table VI. All the flames have burning velocities much lower than those considered in Section 4(a), and, in contrast with the faster flames, the comparison of theory with experiment now reacts to the combined effect of changes in reaction rate parameters *and* changes in the assumed diffusive properties of hydrogen atoms as compared with earlier work. The lines in Figures 2 to 4 show the new profiles of $[OH]^{-1}$, again computed with partial equilibrium assumptions on reactions (i), (ii), (iii) and (xviii), and with use of the parameters from Tables II and IV. Agreement between theory and experiment is satisfactory.

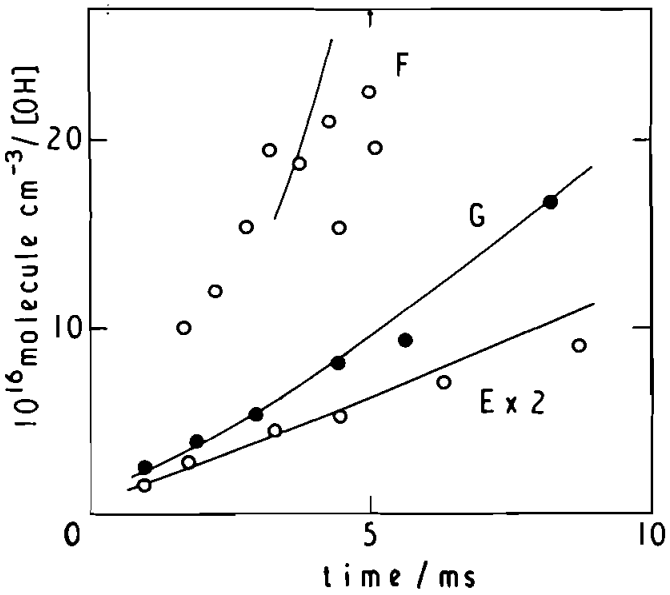

FIGURE 2 Recombination in fuel-rich hydrogen–oxygen–nitrogen flames. Comparison of measured points of Kaskan (1958a) with computed lines. Letters refer to flames of Table VI. Transport and reaction rate parameters from Tables II and IV.

c) *Temperature Dependence of the Diffusion of Atomic Hydrogen*

No direct data are available concerning the diffusion of atomic hydrogen at high temperatures, and the low value of the Lennard-Jones parameter $(eps)_H/k=37.0$ K in Table II is tantamount to assuming interactions with other molecules more or less on a "point centres of repulsion" basis, with the interaction potential ϕ given as a function of intermolecular distance r by:

$$\phi = dr^{-\delta}, \tag{24}$$

and with an index of repulsion $\delta=12$. The assumption leads directly (Hirschfelder

et al., 1954) to a $T^{(1.5+2/\delta)}$ (that is, $=T^{1.67}$) temperature dependence of the diffusion coefficient. The parameters given in Table II lead to $\mathscr{D}_{H,N_2}=1.27\ cm^2\ s^{-1}$ at 294 K and 19.16 $cm^2\ s^{-1}$ at 1500 K, both at a pressure of one atmosphere.

As already mentioned, the measurements of Clifford *et al.* (1982) yielded $\mathscr{D}_{H,N_2}=1.35\pm0.03\ cm^2\ s^{-1}$ at 294 K and 1 atm, a result 6 percent in excess of the above calculated figure. If the mean measured value is combined with $\mathscr{D}_{H,N_2}=19.16\ cm^2\ s^{-1}$ at 1500 K, it leads closely to a $T^{1.625}$ temperature dependence of the diffusion coefficient, corresponding to $\delta=16$. Alternatively, the measured value combined with a $T^{1.60}$ temperature dependence ($\delta=20$) would yield $\mathscr{D}_{H,N_2}=18.32\ cm^2\ s^{-1}$ at 1500 K. Over the more important temperature range for flame calculation, the Lennard-Jones representation of hydrogen atom diffusion in nitrogen, with $\sigma_H=0.225$ nm and $(eps)_H/k=37.0$ K, thus gives a reasonable but slightly skewed fit to a point centre of repulsion model with $\delta=20$. The model corresponds with a rather "hard" hydrogen atom. It is felt that a temperature dependence lower than $T^{1.60}$ is most unlikely, and thus that the hydrogen atom diffusion representation in the flame calculations employs minimum hydrogen atom diffusion coefficients consistent with the recent room temperature measurements.

For the reaction kinetics, the conclusion again is that $A_2<2.2\times10^{14}\ cm^3\ mol^{-1}\ s^{-1}$. Indeed, if the 41 percent hydrogen–air flame properties are computed as in Table III,

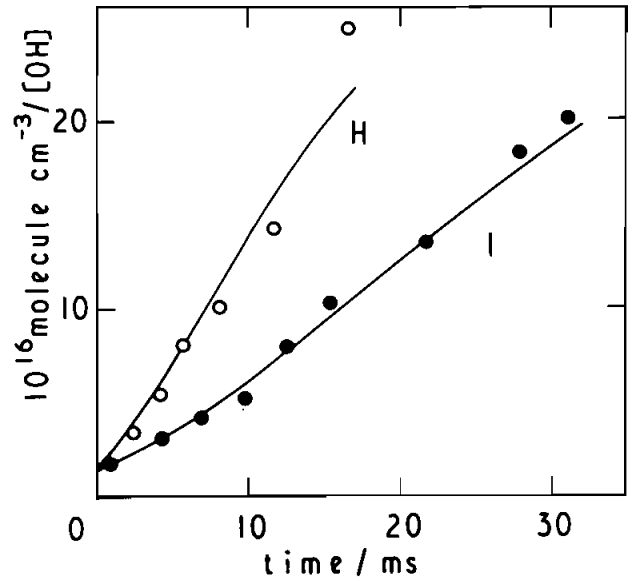

FIGURE 3 Recombination in fuel-lean hydrogen–oxygen–nitrogen flames. Comparison of measured points of Kaskan (1958b) with computed lines. Letters refer to flames of Table VI. Transport and reaction rate parameters from Tables II and IV.

run 12H, but with $\sigma_H=0.207$ nm [cf. Section 3(c)], then the value of A_2 must be reduced to $1.75\times10^{14}\ cm^3\ mol^{-1}\ s^{-1}$ in order to predict a burning velocity of 299.7 cm s^{-1}.

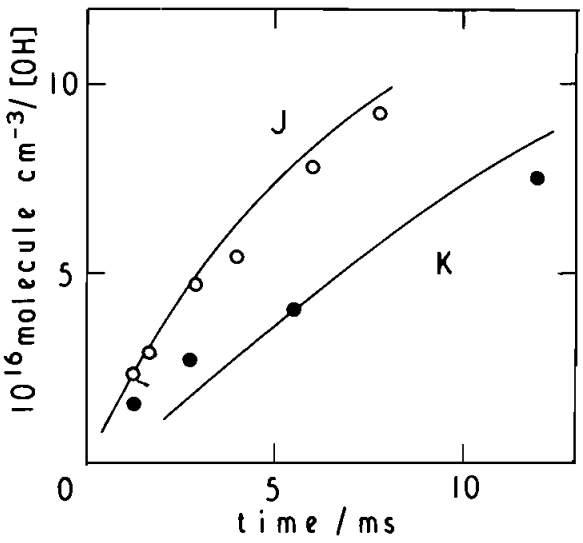

FIGURE 4 Recombination in fuel-lean hydrogen–oxygen–nitrogen flames. Comparison of measured points of Kaskan (1958b) with computed lines. Letters refer to flames of Table VI. Transport and reaction rate parameters from Tables II and IV.

d) *Properties of Low Temperature, Fuel-Rich Flames*

Table VII lists the properties of three low temperature, fuel-rich flames for which the burning velocities have been measured by Day *et al.* (1972). The final two columns of Table VII compare the observed burning velocities with those calculated by use of the parameters of Tables II and IV. Taking account of the somewhat subjective nature of the divergence correction applied by Day *et al.* in the burning velocity measurement, the agreement is good. It is further worth noting here that the sensitivity of the predicted burning velocity of flame *M* to the value of k_2 has been shown (Dixon-Lewis, 1979) to be such that, for a constant ratio $(k_7+k_{7a})/k_{12}$, an increase of 10 percent in the assumed value of A_2 and the related A_4 causes a 6 to 7 percent increase in the velocity.

Two additional computations were performed for flame M, as follows:

i) The conditions for the first trial corresponded with run 8H of Table III, and led to a predicted burning velocity of 8.56 cm s^{-1}, referred to unburnt gas conditions of 291 K/1 atm. By reference to Table III it was therefore concluded that, starting from run 12H as base, upward adjustment of A_2 to 2.2×10^{14} combined with reduction of the ratio $(k_7+k_{7a})/k_{12}$ at 773 K cannot simultaneously accommodate the hydrogen atom diffusion data and the burning velocity requirements of both flame *M* and the 41 percent hydrogen–air flame.

ii) The second trial corresponded with run 12H, but with $\sigma_H=0.207$ nm and $A_2=1.75\times10^{14}$ cm^3 mol^{-1} s^{-1} as at the end of Section 4(c). The predicted burning velocity was 9.36 cm s^{-1}.

Finally with regard to these burning velocities, the points in Figure 5 show measurements for a series of hydrogen–oxygen–nitrogen flames similar to those of Table VII,

with $X_{O_2,u}=0.0460$ and $T_u=336$ K, and with varying ratio $X_{H_2,u}/X_{N_2,u}$. The line is constructed from the three computed burning velocities given in Table VII.

TABLE VII
Initial compositions, flame temperatures and burning velocities of low temperature flames at atmospheric pressure. (In all cases initial temperature $T_u=336$ K)

Flame	$X_{H_2,u}/X_{N_2,u}$	$X_{H_2,u}$	$X_{N_2,u}$	$X_{O_2,u}$	T_b/K	$S_{u,obs}$/(cm s^{-1})[a]	$S_{u,calc}$/(cm s^{-1})[a]
L	0.141	0.1181	0.8359	0.0460	1076	6.5±0.2	6.95
M	0.246	0.1883	0.7657	0.0460	1078	9.2±0.2	9.85
N	0.372	0.2587	0.6953	0.0460	1080	11.0±0.2	11.55

[a]Quoted on basis of unburnt gases at 291 K and 1 atm pressure, for these three flames only.

A more stringent test of the proposed set of transport and raction rate parameters lies in the satisfactory prediction of the hydrogen atom profiles in the flames. For flame *M*, Dixon-Lewis *et al.* (1965) measured the profile of the mole fraction ratio X_{CO_2}/X_{N_2} when a trace of carbon dioxide was added to the entering gases. The measurements are shown as the points in Figure 6. The attack on the carbon dioxide is by reaction (-xxi):

$$OH + CO \rightleftharpoons CO_2 + H, \qquad \text{(xxi)}$$

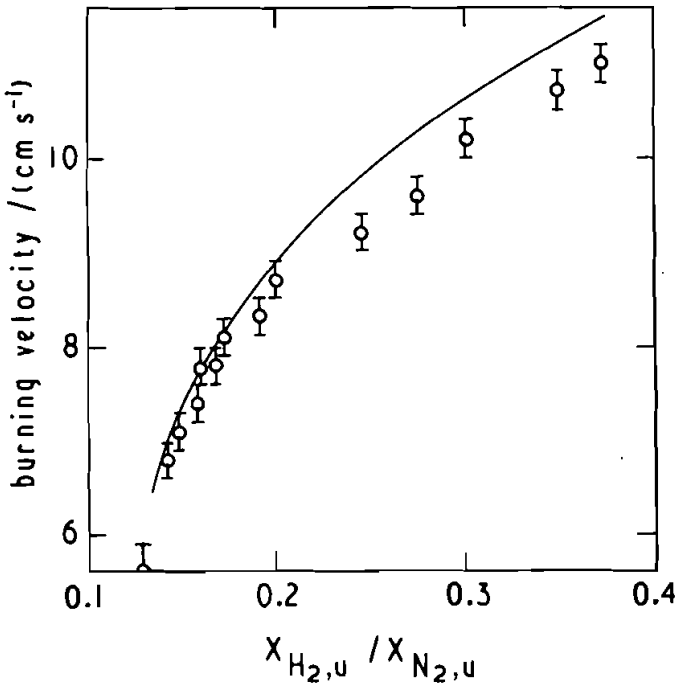

FIGURE 5 Burning velocities of hydrogen–oxygen–nitrogen flames having $X_{O_2,u}=0.0460$ and $T_u=336$ K, showing dependence on the initial mole fraction ratio $X_{H_2,u}/X_{N_2,u}$, and comparing observed values of Day *et al.* (1972) with line computed using transport and reaction rate parameters from Tables II and IV. Burning velocities in this Figure are on basis of unburnt gas at 291 K/1 atm.

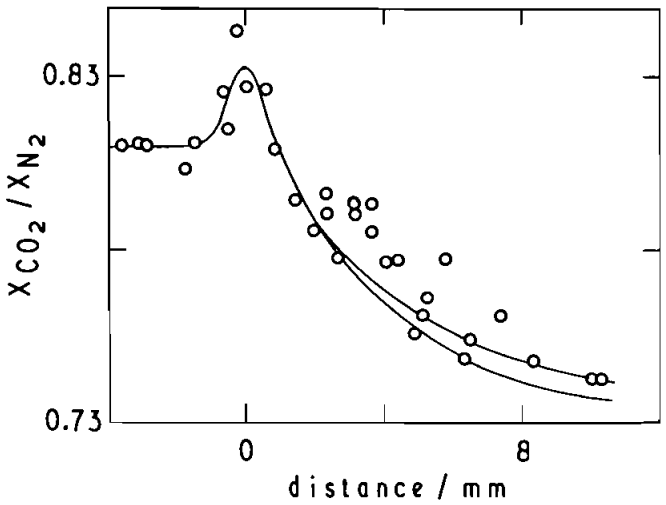

FIGURE 6 Disappearance of carbon dioxide in flame having initial mole fraction composition $X_{H_2,u}=0.1883$, $X_{O_2,u}=0.0462$, $X_{N_2,u}=0.7594$ and $X_{CO_2,u}=0.0061(5)$ at atmospheric pressure, with $T_u=336$ K, showing comparison between computed lines and experimental points. Transport and reaction rate parameters from Tables II and IV. Lower line: $k_{21}=1.5\times10^7\ T^{1.3}\exp(+385/T)$; upper line: $k_{21}=1.35\times10^7\ T^{1.3}\exp(+385/T)$ cm^3 mol^{-1} s^{-1}. Computed burning velocity $S_u=9.7$ cm s^{-1}, quoted for unburnt gas at 291 K/1 atm.

and analysis of the flame profiles with the use of the mean rate expression $k_{21}=1.5\times10^7\ T^{1.3}\exp(+385/T)$ cm^3 mol^{-1} s^{-1} recommended by Baulch and Drysdale (1974) led to $X_{H,max}=1.48\times10^{-3}$ (see Dixon-Lewis, 1979; Cherian *et al.*, 1981). The initial computation for flame *M* with the diffusion and reaction rate parameters from Tables II and IV gave this value precisely. With $\sigma_H=0.207$ nm and $A_2=1.75\times10^{14}$, $X_{H,max}$ was slightly lower, at 1.42×10^{-3}.

A re-computation of the flame with the trace addition of carbon dioxide was also carried out with the use of the tabulated new parameters. With k_{21} given by the mean expression above, the computation led to the X_{CO_2}/X_{N_2} profile shown by the lower line in Figure 6. A 10 percent reduction in k_{21} from the mean expression led to the upper line. Clearly the parameters of Tables II and IV, and the slightly lower σ_H and A_2 introduced at the end of Section 4(c), are both entirely consistent with this calibration experiment.

e) *Further Consideration of Burning Velocity of 41 percent Hydrogen–Air Flame, and Comments on the Optimum Expression for the Reaction Rate Coefficient* k_2

Lastly, returning to the 41 percent hydrogen–air flame, a repetition of run 12H of Table III, but with increases of 20 percent in all the hydrogen atom recombination rate coefficients k_{15} above the values of Table IV, caused the predicted burning velocity decrease from 300 to 298 cm s^{-1}. The reduction may be compensated for by an increase in A_2, but the sensitivity of the optimum A_2 to the value of k_{15} is clearly small. Based on the activation energy $E_2=70.3$ kJ mol^{-1}, the overall sensitivity investigation strongly supports Eq. (25):

$$k_2 = (1.8\pm0.2)\times10^{14}\exp(-8450/T)\ \text{cm}^3\ \text{mol}^{-1}\ \text{s}^{-1} \qquad (25)$$

as an optimum two-parameter expression in the temperature range 700 to 1500 K. Lower assumed activation energies E_2=67.3 and 68.6 kJ mol^{-1} would lead to the *mean* expressions (26) and (26a):

$$k_2 = 1.2 \times 10^{14} \exp(-8100/T) \tag{26}$$

$$k_2 = 1.4 \times 10^{14} \exp(-8250/T) \tag{26a}$$

Equation (26a) is almost identical with the expression for k_2 recommended by Dixon-Lewis and Williams (1977).

It should be noted here that because the free radical production region in any specific flame extends over a considerable temperature range, it is not possible to use the macroscopic flame properties to define the activation energy E_2 very closely. Below about 700 K the values of k_2 become too small compared with k_4 for the flame properties to be directly affected by their magnitude. However, at 773 K the magnitude of k_2 is fixed rather closely by its relationship with k_4 (Table I), and the governance of the lean flame recombination by k_4, as outlined in Section 4(a). At higher temperatures in the reaction zones, the maximum net rates of formation of radicals occur between 1100 and 1450 K, depending on the flame. Then, later still in the reaction zones, Dixon-Lewis (1979) found that above about 1260 K in the 70 percent hydrogen–air flame, or above 1550 to 1650 K in the other flames, the partial equilibrium situation is established in which reactions (i), (ii) and (iii) are all effectively equilibrated. Provided that k_2 is large enough to maintain the close approximation to partial equilibrium in the recombination regions of the flames, its precise value does not then influence the computation in a significant manner. The flame properties are thus most sensitive to the expression for k_2 at temperatures between about 700 and 1500 K, as quoted.

The range of values of k_2 given by Eq. (25) is consistent with the expression and error limits recommended by Baulch *et al.* (1972), but the new pre-exponential factor is lower, and the expression itself carries narrower error limits. The Arrhenius activation energy line is slightly steeper than that obtained by Schott (1973) from analysis of a large number of shock tube results, with k_2 some 10 percent lower than Schott's value at 1250 K, and 5 percent higher at 1500 K. Schott's mean expression, for the temperature range 1250 to 2500 K, is:

$$k_2 = 1.22 \times 10^{17} T^{-0.907} \exp(-8369/T). \tag{27}$$

Equations (26) and (26a) give the same k_2 as Schott at 1700 and 1600 K respectively, and the two activation energy lines in the temperature range 1150 to 1600 K lie below the results of Schott on the one hand, and between 2 and 7 percent above the shock tube results of Brabbs, Belles and Brokaw (1971) on the other. Equation (26) gives k_2 uniformly some 10 percent higher than the expression $k_2 = 1.1 \times 10^{14} \exp(-8100/T)$ given by Chiang and Skinner (1979). The expressions of Brabbs *et al.* (1971) and Chiang and Skinner (1979) both give $k_2 = 3.1 \times 10^9$ cm^3 mol^{-1} s^{-1} at 773 K.

Miller (1981) has recently predicted an expression for k_2 theoretically by means of classical trajectory calculations. He obtained:

$$k_2 = 5.13 \times 10^{16} T^{-0.816} \exp(-8306/T). \tag{28}$$

The temperature dependence is similar to that found experimentally by Schott (1973), but the absolute values of k_2 are some 15 to 18 percent lower. Agreement with the flame model expressions (25) and (26) is good at temperatures between 1250 and 1500 K. However, neither of the expressions (27) or (28) is compatible with the

requirements of the flame model at 773 K. At this temperature Eq. (27) predicts a value of k_2 some 80 percent higher than that obtained from either of the two-parameter relations (25) or (26). Taking cognizance of both the flame results and the three sets of shock tube data quoted, retention of the activation energy $E_2=70.3$ kJ mol^{-1} in a three-parameter, modified Arrhenius expression for k_2 leads to either:

$$k_2 = 4.2 \times 10^{15} T^{-0.46} \exp(-8450/T) \tag{29}$$

or

$$k_2 = 7.8 \times 10^{15} T^{-0.55} \exp(-8450/T) \text{ cm}^3 \text{ mol}^{-1} \text{ s}^{-1} \tag{29a}$$

as a good parametric fit over the temperature range 700 to 2500 K. Both expressions have confidence limits of ± 10 percent. At 2500 K the two equations give $k_2=3.9\times10^{12}$ and 3.6×10^{12} respectively. At the lower end of the temperature range, both are in excellent agreement with the results of Karmilova, Nalbandjan and Semenov (1958); whilst on extrapolation down to 300 K they yield $k_2=179$ and 199 cm^3 mol^{-1} s^{-1} respectively. Combination with the equilibrium constant $k_2=1.0\times10^{-11}$ at 300 K then leads to $k_{-2}=1.79\times10^{13}$ or 1.99×10^{13}, just 25 percent (or 15 percent) lower than the mean k_{-2} given by Baulch *et al.* (1972) and recently confirmed by Howard and Smith (1980).

One further feature of the flame kinetic model needs examination in relation to these expressions for k_2. It is that whereas Table IV assumes temperature independent values for the various chaperon efficiencies in reaction (iv), the review by Dixon-Lewis and Williams (1977) of the then available data led to $k_{4,N_2}/k_{4,H_2}=134T^{-0.86}$. Taking $k_{4,O_2}/k_{4,H_2}=107T^{-0.86}$ and $k_{4,N_2}/k_{4,H_2}=134T^{-0.86}$, and adjusting A_{4,H_2}, A_{7+7a} and A_{12} so that the corresponding rate coefficients at 773 K conform with both Table I and Eq. (29), the high temperature, lean flame recombination results of Friswell and Sutton (1972) (see Figure 1) lead, in combination with $k_{4,H_2O}/k_{4,H_2}=6.5$ at 773 K, to the expression $k_{4,H_2O}/k_{4,H_2}=3.35T^{0.1}$. Complete flame computations using the new set of expressions for the efficiencies then lead [with $\sigma_H=0.207$ nm and k_2 from Eq. (29)] to burning velocities of 300 cm s^{-1} for the 41 percent hydrogen–air flame at atmospheric pressure, and 9.2 cm s^{-1} (quoted for unburnt gas at 291 K/1 atm) for flame *M* of Table VII, and to a maximum hydrogen atom mole fraction $X_H=1.33\times10^{-3}$ in the latter flame. The agreement with experiment is excellent, and further confirms that the optimum expression for k_2 is close to those given in Eqs. (29) and (29a).

5 PREDICTION OF SPHERICAL FLAME SPEEDS ACROSS THE WHOLE FLAMMABLE RANGE OF HYDROGEN-AIR MIXTURES

To supplement the investigations already outlined, the computational technique described in Section 2 was used to derive the spherical flame speeds of eight further hydrogen–air mixtures at atmospheric pressure, all with $T_u=298$ K, but having respectively $X_{H_2,u}=0.70$, 0.60, 0.50, 0.41, 0.35, 0.30, 0.25, 0.20 and 0.15. The transport and reaction rate parameters from Tables II and IV were again used, and the computations were arranged so that the steady flame speed was achieved at a flame radius as near as possible to 25 mm. This facilitates comparison with the experimental observations of Andrews and Bradley (1973).

Table VIII summarizes a few of the more important flame properties which emerge

TABLE VIII

Predicted properties of hydrogen–air flames with $T_u = 298$ K at atmospheric pressure. (Transport parameters from Table II. Reaction rate parameters from Table IV)

$X_{H_2,u}$	0.70	0.60	0.50	0.41	0.35	0.30	0.25	0.20	0.15
$T_{b,equil}$/K	1328	1644	1941	2191		2401	2171	1836	1472
T_{centre}/K	1325	1627	1911	2150	2307	2360	2155	1832	1472
$S_{u,planar}$/(cm s^{-1})	90.2	192.4	271.5	300.0	277.7	232.3	167.9	93.0	30.2
$10^2 X_{H\ max,\ planar}$[a]	1.239	3.590	6.189	7.508	6.539	4.692	2.675	1.038	0.179
At T/K[a]	1193	1341	1450	1546	1571	1540	1470	1380	1235
S_s/(cm s^{-1})	297	894	1450	1778	1758	1485	1012	580	169
$10^2 X_{H\ max,\ spher}$[a]	1.000	3.443	5.973	7.418	6.422	4.591	2.584	1.280	0.24
At T/K[a]	1168	1339	1444	1536	1565	1534	1458	1400	1276
[b]$S_{u,\ spher}$/(cm s^{-1})	75	184	262	290	273	227	163	106	36.3

[a]These maxima and temperatures are somewhat approximate (*ca.* 1% for $X_{H,\ max}$ and $\pm 10°$ for T) because of finite difference nature of calculation.
[b]Values of $S_{u,\ spher}$ are calculated at a flame radius of approximately 25 mm (see Section 2(f) and Section 6).

from the computations for all the hydrogen–air flames, including both (i) the planar burning velocities $S_{u,\text{planar}}$ which derive from the initial Eulerian procedure for each flame (see Section 2), and (ii) the final Lagrangian steady state spherical flame speeds S_s. Also given in Table VIII are (iii) the adiabatic equilibrium flame temperatures $T_{b,\text{equil}}$ of the mixtures, and (iv) the temperatures T_{centre} at the centre of the spherical core of burnt gas when the flame is at a radius of 25 mm. The temperature shortfall in the spherical core, which increases on moving away from the centre, is due to the slow rate of heat release by recombination steps when the radical concentration is low. The shortfall was misinterpreted by earlier workers as being due to high radiative losses. Its existence also means that, for good accuracy, some care must be taken realistically to model the recombination regions of the flames.

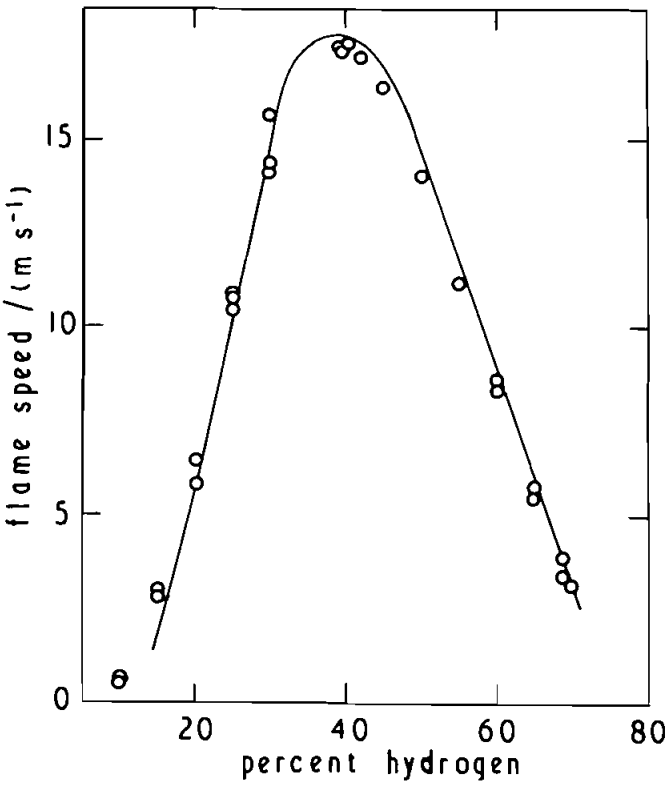

FIGURE 7 Spherical flame speeds of hydrogen–air mixtures, comparing computed line with measurements of Andrews and Bradley (1973). Transport and reaction rate parameters for computation from Tables II and IV.

Lastly, the points in Figure 7 show the spherical flame speeds in hydrogen–air mixtures at atmospheric pressure, as measured by Andrews and Bradley (1973). The line represents the computed results. The agreement is within the experimental error over almost the whole flammable range, and remains reasonable well on the fuel-lean side of stoichiometric, despite the appearance of cellular flames there. Andrews and Bradley report the limit for the appearance of cellular flames at about 25 percent hydrogen.

6 BURNING VELOCITIES AND OTHER PROPERTIES OF FLAMES

Independently of some of the finer detail of the kinetic mechanism, the agreement between the predicted and measured flame speeds, as shown in Figure 7, implies that the directly computed planar burning velocities $S_{u,\text{planar}}$ given in Table VIII are accurate to within a percent or so, that is, to within the accuracy of the *objective* flame speed measurements. By using the methods of Section 2(f), it is also possible to determine the effective burning velocities at several positions within the spherically propagating flames. When reduced to unburnt gas conditions, the linear burning velocities deduced in this way for different planes in the same spherical flame agree to better than 1 percent. However, they differ from the planar burning velocity for the same mixture. Burning velocities $S_{u,\text{sphere}}$, calculated by the method of Section 2(f) for the steadily propagating spherical flames at a radius near 25 mm, are given as the last line in Table VIII. Effects of flame curvature on the burning velocity, as

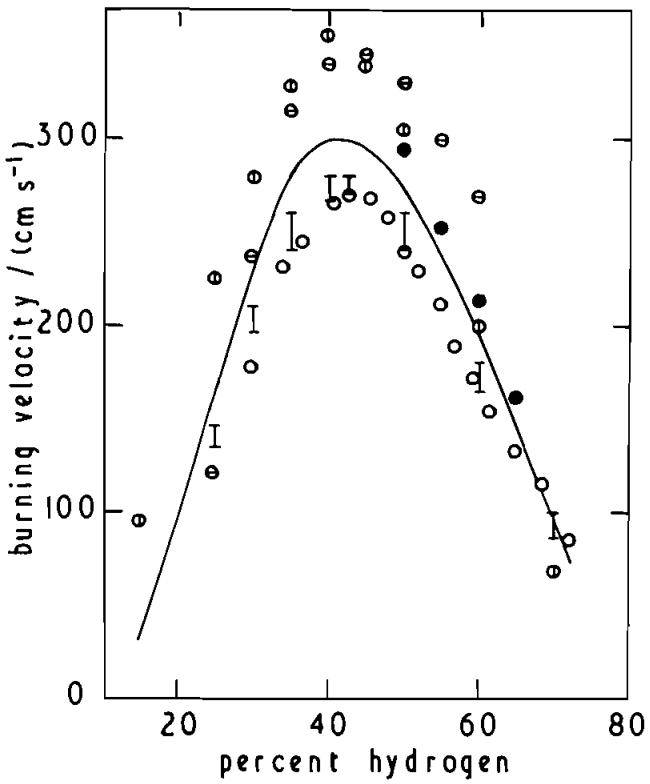

FIGURE 8 Planar burning velocities of hydrogen–air mixtures, comparing reference line computed from parameters of Tables II and IV with some published measurements by burner methods: ○, Jahn (1934); I, Scholte and Vaags (1959); ●, Edmondson and Heap (1971); ⊖, Günther and Janisch (1971); ⊙, Günther and Janisch (1972).

revealed by comparison of $S_{u,\text{planar}}$ with $S_{u,\text{sphere}}$, are never quite absent, but they become particularly noticeable towards the extremities of the flammable range. They are almost certainly connected with (i) flame stretch effects (on the fuel-rich side of stoichiometric where the spherical burning velocity is below the planar), or (ii) effects due to preferential inward diffusion of molecular hydrogen (in fuel-lean flames, where the lean mixtures can become enriched in hydrogen in this way). There is also some evidence that the effects are larger at smaller flame kernel diameters, but consideration of these effects and the small modifications of flame structure which occur during spherical propagation will be postponed until a later paper. The complexities of the situation make it appear virtually impossible reliably to convert constant volume bomb, pre-pressure period, spherical flame speeds into planar, laminar, one-dimensional burning velocities without calibration by kinetic investigation and computation. On the other hand, because of the less easily defined aerodynamic features of burner flames, the spherical flame speed measurements offer a much more objective approach to flame velocity determination than do direct burning velocity measurements on stationary flames. By way of illustration of this last point, Figure 8 compares the burning velocities $S_{u,\text{planar}}$ from Table VIII with the results of several careful direct observations by burner methods.

REFERENCES

Andrews, G. E., and Bradley, D. (1973). Determination of burning velocity by double ignition in a closed vessel. *Combustion and Flame* **20,** 77.

Baldwin, R. R., Fuller, M. E., Hillman, J. S., Jackson, D., and Walker, R. W. (1974). Second limit of hydrogen+oxygen mixtures: the reaction $H+HO_2$. *J. Chem. Soc. Faraday Trans. I* **70,** 635.

Baulch, D. L., Drysdale, D. D., Horne, D. G., and Lloyd, A. C. (1972). *Evaluated Kinetic Data for High Temperature Reactions*, vol **1.** Butterworths, London.

Baulch, D. L., and Drysdale, D. D. (1974). An evaluation of the rate data for the reaction $CO+OH\rightarrow CO_2+H$. *Combustion and Flame* **23,** 215.

Bishop, W. P., and Dorfman, L. M. (1970). Pulse radiolysis studies XVI. Kinetics of the reaction of gaseous hydrogen atoms with molecular oxygen by fast Lyman-α absorption spectroscopy. *J. Chem. Phys.* **52,** 3210.

Bledjian, L. (1973). Computation of time-dependent laminar flame structure. *Combustion and Flame* **20,** 5.

Brabbs, T. A., Belles, F. E., and Brokaw, R. S. (1971). Shock tube measurements of specific reaction rates in the branched-chain H_2–CO–O_2 system. *Thirteenth Symposium (International) on Combustion*, The Combustion Institute, Pittsburgh. p. 129.

Cherian, M. A., Rhodes, P., Simpson, R. J., and Dixon-Lewis, G. (1981). Structure, chemical mechanism and properties of premixed flames in mixtures of carbon monoxide, nitrogen and oxygen with hydrogen and water vapour. *Phil. Trans. Roy. Soc. Lond. A* **303,** 181.

Chiang, C.-C., and Skinner, G. B. (1980). Resonance absorption mesaurements of atom concentrations in reacting gas mixtures. 4. Measurements of hydrogen and deuterium atoms in oxidation of hydrogen, deuterium and methane-D_4. In Lifshitz, A. (Ed.), *Proc. Twelfth International Shock Tube Symposium*, Josef Magnes Press, Hebrew University, Jerusalem. p. 629.

Clifford, A. A., Gray, P., Mason, R. S., and Waddicor, J. I. (1982). Measurement of the diffusion coefficients of reactive species in dilute gases. *Proc. Roy. Soc. Lond. A* **380,** 241.

Clyne, M. A. A., and Thrush, B. A. (1963). Rates of elementary processes in the chain reaction between hydrogen and oxygen. II. Kinetics of the reaction of hydrogen atoms with molecular oxygen. *Proc. Roy. Soc. Lond. A* **275,** 559.

Day, M. J., Dixon-Lewis, G., and Thompson, K. (1972). Flame structure and flame reaction kinetics. VI. Structure, mechanism and properties of rich hydrogen+nitrogen+oxygen flames. *Proc. Roy. Soc. Lond. A* **330,** 199.

Dixon-Lewis, G. (1968). Flame structure and flame reaction kinetics. II. Transport phenomena in multocomponent systems. *Proc. Roy. Soc. Lond. A* **307,** 111.

Dixon-Lewis, G. (1978). Effect of core size on ignition energy by localized sources. *Combustion and Flame* **33**, 319.

Dixon-Lewis, G. (1979). Kinetic mechanism, structure and properties of premixed flames in hydrogen–oxygen–nitrogen mixtures. *Phil. Trans. Roy. Soc. Lond. A* **292**, 45.

Dixon-Lewis, G. (1983). Computer modelling of combustion reactions in flowing systems with transport. In Gardiner, W. C. (Ed.), *Chemical Kinetics of Combustion Reactions*, Springer-Verlag, New York. In press.

Dixon-Lewis, G., Goldsworthy, F. A., and Greenberg, J. B. (1975). Flame structure and flame reaction kinetics. IX. Calculation of properties of multiradical premixed flames. *Proc. Roy. Soc. Lond. A* **346**, 261.

Dixon-Lewis, G., and Islam, S. M. (1982). Flame modelling and burning velocity measurement. *Nineteenth Symposium (International) on Combustion*, The Combustion Institute, Pittsburgh. p. 283.

Dixon-Lewis, G., and Shepherd, I. G. (1974). Some aspects of ignition by localized sources, and of cylindrical and spherical flames. *Fifteenth Symposium (International) on Combustion*, The Combustion Institute, Pittsburgh. p. 1483.

Dixon-Lewis, G., Sutton, M. M., and Williams, A. (1965). Reactions contributing to the establishment of the water–gas equilibrium when carbon dioxide is added to a hydrogen–oxygen flame. *Trans. Faraday Soc.* **61**, 255.

Dixon-Lewis, G., and Williams, D. J. (1977). The oxidation of hydrogen and carbon monoxide. In Bamford, C. H. and Tipper, C. F. H. (Eds.), *Comprehensive Chemical Kinetics*, Elsevier, Amsterdam, vol **17**, Chap 1, pp. 1–248.

Edmondson, H., and Heap, M. P. (1971). The burning velocity of hydrogen–air flames. *Combustion and Flame* **16**, 161.

Friswell, N. J., and Sutton, M. M. (1972). Radical recombination reactions in $H_2/O_2/N_2$ flames: participation of the HO_2 radical. *Chem. Phys. Lett.* **15**, 108.

Günther, R., and Janisch, G. (1971). Messwerte der Flammengeschwindigkeit von Gasen und Gasgemischen. *Chem.-Ing.-Techn.* **43**, 975.

Günther, R., and Janisch, G. (1972). Measurement of burning velocity in a flat flame front. *Combustion and Flame* **19**, 49.

Hack, W., Wagner, H.Gg., and Hoyermann, K. (1978). Reaktionen von Wasserstoffatomen mit Hydroperoxylradikalen. I. Bestimmung der spezifischen Geschwindigkeitskonstanten der Reaktionskanäle. *Ber. der Bunsenges. phys. Chem.* **82**, 713.

Hack, W., Preuss, A. W., Wagner, H.Gg., and Hoyermann, K. (1979). Reaktionen von Wasserstoffatomen mit Hydroperoxylradikalen. II. Bestimmung der Geschwindigkeitskonstanten der Bruttoreaktion. *Ber. der Bunsenges. phys. Chem.* **83**, 212.

Hack, W., Preuss, A. W., and Wagner, H.Gg. (1978). Messungen der Geschwindigkeit der Reaktionen von OH under HO_2-Radikalen mit Hilfe der Laser-Magnetischen Resonanz. *Ber. der Bunsenges. phys. Chem.* **82**, 1167.

Hack, W., Preuss, A. W., Temps, F., and Wagner, H.Gg. (1979). The reaction $O + HO_2 \rightarrow OH + O_2$ studied with a L.M.R.–E.S.R. spectrometer. *Ber der Bunsenges. phys. Chem.* **83**, 1275.

Hirschfelder, J. O., Curtiss, C. F., and Bird, R. B. (1954). *Molecular Theory of Gases and Liquids*, John Wiley and Sons, New York. p. 547.

Howard, M. J., and Smith, I. W. M. (1980). Direct rate measurements on the reactions $N + OH \rightarrow NO + H$ and $O + OH \rightarrow O_2 + H$. *Chem. Phys. Lett.* **69**, 40.

Jahn, G. (1934). *Der Zündvorgang in Gasgemischen*, Oldenbourg, Berlin.

Karmilova, L. V., Nalbandjan, A. B., and Semenov, N. N. (1958). Hydrogen combustion kinetics with oxygen below the lower autoignition temperature. *Zhur. Fiz. Khim.* **32**, 1193.

Kaskan, W. E. (1958a). Hydroxyl concentrations in rich hydrogen–air flames held on porous burners. *Combustion and Flame* **2**, 229.

Kaskan, W. E. (1958b). The concentration of hydroxyl and of oxygen atoms in gases from lean hydrogen–air flames. *Combustion and Flame* **2**, 286.

Mason, E. A., and Monchick, L. (1962). Heat conductivity of polyatomic and polar gases. *J. Chem Phys.* **36**, 1622.

Miller, J. A. (1981). Collision dynamics and the thermal rate coefficient for the reaction $H + O_2 \rightarrow OH + O$. *J. Chem. Phys.* **74**, 5120.

Monchick, L., and Mason, E. A. (1961). Transport properties of polar gases. *J. Chem. Phys.* **35**, 1676.

Monchick, L., Munn, R. J., and Mason, E. A. (1966). Thermal diffusion in polyatomic gases: a generalized Stefan–Maxwell diffusion equation. *J. Chem. Phys.* **45**, 3051.

Monchick, L., Pereira, A. N. G., and Mason, E. A. (1965). Heat conductivity of polyatomic and polar gases and gas mixtures. *J. Chem. Phys.* **42,** 3241.

Monchick, L., Yun, K. S., and Mason, E. A. (1963). Formal kinetic theory of transport phenomena in polyatomic gas mixtures. *J. Chem. Phys.* **39,** 654.

Moortgat, G. K., and Allen, E. R. (1972). Paper presented at 163rd Am. Chem. Soc. National Meeting, Boston, Mass.

Overley, J. R., Overholser, K. A., and Reddien, G. W. (1978). Calculation of minimum ignition energy and time-dependent laminar flame profiles. *Combustion and Flame* **31,** 69.

Patankar, S. V., and Spalding, D. B. (1970). *Heat and Mass Transfer in Boundary Layers*, 2nd. ed., Intertext Books, London, pp. 92–95.

Richtmyer, R. D., and Morton, K. W. (1967). *Difference Methods for Initial Value Problems*, 2nd. ed., John Wiley and Sons, New York, p. 199.

Roache, P. J. (1972). *Computational Fluid Dynamics*, Hermosa Publishers, Albuquerque, N.M., p. 345.

Scholte, T. G., and Vaags, P. B. (1959). The burning velocity of hydrogen–air mixtures and mixtures of some hydrocarbons with air. *Combustion and Flame* **3,** 495.

Schott, G. L. (1973). Further studies of exponential branching rates in reflected-shock heated, non-stoichiometric H_2–CO–O_2 systems. *Combustion and Flame* **21,** 357.

Spalding, D. B., and Stephenson, P. L. (1971). Laminar flame propagation in hydrogen + bromine mixtures. *Proc. Roy. Soc. Lond. A* **324,** 315.

Spalding, D. B., Stephenson, P. L., and Taylor, R. G. (1971). A calculation procedure for the prediction of laminar flame speeds. *Combustion and Flame* **17,** 55.

Stephenson, P. L., and Taylor, R. G. (1973). Laminar flame propagation in hydrogen, oxygen, nitrogen mixtures. *Combustion and Flame* **20,** 231.

Svehla, R. A. (1962). Estimated viscosities and thermal conductivities of gases at high temperatures. *NASA Tech. Rep.* R-132, Washington, D.C.

Tsatsaronis, G. (1978). Prediction of propagating flames in methane, oxygen, nitrogen mixtures. *Combustion and Flame* **33,** 217.

Warnatz, J. (1978). Calculation of the structure of laminar flat flames. II. Flame velocity and structure of freely propagating hydrogen–oxygen and hydrogen–air flames. *Ber. der Bunsenges. phys. Chem.* **82,** 643.

Warnatz, J. (1981). Concentration, pressure, and temperature dependence of the flame velocity in hydrogen–oxygen–nitrogen mixtures. *Combustion Science and Technology* **26,** 203.

Wong, W., and Davis, D. D. (1974). A flash photolysis–resonance fluorescence study of the reaction of atomic hydrogen with molecular oxygen $H + O_2 + M \rightarrow HO_2 + M$. *Int. J. Chem. Kinet.* **6,** 401.